Direct Bonding of Aluminum–Copper Metals through High-Pressure Torsion Processing

Jae-Kyung Han, Dae Kuen Han, Guang Yuan Liang, Jae-Il Jang,*
Terence G. Langdon, and Megumi Kawasaki*

High-pressure torsion (HPT) is used to investigate the formation of a new metal system by the direct bonding of separate disks of Al and Cu by processing at room temperature under a compressive pressure of 6.0 GPa and with increasing numbers of HPT turns up to 60. A detailed examination of the microstructure and a phase analysis reveal the presence of three intermetallic compounds, Al_2Cu, $AlCu$, and Al_4Cu_9, in the nanostructured Al matrix with a grain size of ≈ 30 nm. Processing by HPT leads to the formation of a metal–matrix nanocomposite with extreme hardness near the edge of the Al–Cu disks after 60 HPT turns. Experiments show that the estimated wear rates exhibit an improvement in wear resistance while maintaining low wear rates for high applied loads up to ≈ 40–50 N under dry sliding conditions. The results confirm that there is a significant potential for using HPT processing in the joining and bonding of dissimilar metals at room temperature and in the expeditious fabrication of a wide range of new metal systems having enhanced mechanical and functional properties.

1. Introduction

The application of severe plastic deformation (SPD) techniques is a promising approach for achieving significant grain refinement leading to the introduction of ultrafine-grained (UFG) microstructures in bulk metals.[1] A growing interest has arisen in this research field over the last two decades and the UFG metals processed by SPD are now referred to as interface-controlled materials where the grain boundaries are spatially arranged during severe straining.[2] These SPD-processed UFG metals generally exhibit significant superior mechanical and functional properties.

Among the SPD techniques available to date, one of the most attractive methods is processing by high-pressure torsion (HPT).[3] In this procedure, a bulk metal in a disk shape is severely deformed under extreme pressure with concurrent torsional straining and the processing generally introduces exceptional grain refinement that cannot be attained using other SPD procedures.[4] The HPT technique has been successfully utilized for grain refinement by processing at room temperature (RT) for a wide variety of materials including hard-to-deform metal phases such as bulk intermetallic compounds.[5–10] Thus, HPT is a top-down approach[11] in which grain refinement is achieved in bulk solids through the intensive introduction of point and line defects during processing. The basic principles of HPT have been utilized also for the bonding of machining chips[12,13] and the consolidation of metallic powders[14–19] but these processes generally have additional requirements such as a high processing temperature and/or cold/hot compaction prior to the application of HPT.

Responding to current demands for introducing functional metal formation and developing new engineering manufacturing processes, an alternative approach was studied recently by utilizing conventional HPT processing for the direct mechanical bonding of bulk metals through the synthesis of hybrid metal systems. In practice, a first report demonstrated a solid-state reaction by the processing by HPT of commercial purity Al and Cu disks having a semi-circular shape at ambient temperature for up to 100 turns[20] and a similar approach was applied for the formation of a spiral texture by processing of an Al–Cu hybrid material by HPT where four quarter-disks, two of pure Cu and two of an Al-6061 alloy, were positioned to make a complete disk and then processed at RT for 1 turn.[21] Thereafter, HPT processing was applied at RT for the bonding of separate Al and Mg disks through the stacking of two disks for up to 20 turns[22] and the stacking of three disks in the order of Al/Mg/Al for 5–20

Prof. M. Kawasaki, J.-K. Han, G. Y. Liang
School of Mechanical, Industrial and Manufacturing Engineering
Oregon State University
Corvallis OR 97331-6001, USA
E-mail: megumi.kawasaki@oregonstate.edu

Prof. J.-I. Jang, D. K. Han
Division of Materials Science and Engineering
Hanyang University
Seoul 04763, Republic of Korea
E-mail: jijang@hanyang.ac.kr

Prof. M. Kawasaki, D. K. Han
HYU-HPSTAR-CIS High Pressure Research Center
Hanyang University
Seoul 04763, Republic of Korea

Prof. T. G. Langdon
Materials Research Group
Department of Mechanical Engineering
University of Southampton
Southampton SO17 1BJ, UK

turns[23–26] in order to produce bi-layered and multi-layered structures, respectively. This strategy of bonding and mixing dissimilar metals by HPT was further expanded recently to a set of alternately stacked 19 Cu and 18 Ta thin foils to form a bulk solid under pressure for up to 150 turns.[27]

Based on these early results, the present study was initiated to evaluate the potential for making use of HPT at ambient temperature for synthesizing a new Al–Cu alloy system by stacking of metal disks. In this comprehensive study, it is shown that the microstructural and compositional changes lead to hardness variations with increasing straining by increasing the HPT rotations. The wear resistance was examined in detail because this is a critical functionality of engineering materials. The results from this investigation are designed to expand the capability of HPT processing from intensive grain refinement to the preparation of hybrid alloy systems having unique microstructural features which will enhance the physical and mechanical properties of the processed bulk nanomaterials.

2. Experimental materials and procedure

The experiments were conducted by using two conventional engineering metals of a commercial purity (CP) Al (Al-1050) and a CP Cu. A plate of CP Al with a thickness of 1.2 mm was cut into disks with diameters of ≈10 mm by electric discharge machining. The CP Cu was received as extruded bars having diameters of ≈10 mm and these bars were sliced into disks with thicknesses of ≈1.2 mm. The sliced disks of the CP Cu were annealed at 673 K for 1 h for homogenization and the CP Al and Cu disks were then polished to final parallel thicknesses of ≈0.95 mm and ≈0.83 mm, respectively. These different thicknesses of the Al and Cu metal disks were selected after a number of careful trials in order to avoid any slippage between the disks and the anvils. It is reasonable to note that an example of successful sold state reaction of Al and Cu plates was presented earlier by accumulative roll bonding processing when applying a hard phase of Cu in the form of a thin plate between soft phases of Al in the form of thicker plates.[28]

Direct bonding of the CP Al and Cu disks was achieved using a unique sample set-up[23–26] in conventional HPT[29] with a quasi-constrained HPT facility in which there is a small outflow of material around the periphery of the sample during processing.[30] The HPT was conducted under an imposed hydraulic pressure of 6.0 GPa at RT for totals of 10, 20, 40, and 60 turns at a rotational speed of 1 rpm. The individual Al and Cu disks were placed in the depression on the lower anvil of the HPT facility in the order of Al/Cu/Al without any glue or metal brushing between the disks. For comparison purposes, separate disks of CP Al and Cu were processed separately by HPT for 10 turns under the same processing conditions. The processed disks were cut vertically along the diameters to give two semi-circular disks and a vertical cross-section on each processed disk was polished and examined by optical microscopy. Vickers microhardness measurements were taken using a Mitsutoyo HM-200 facility with a load of 50 gf and a dwell time of 10 s. The Vickers microhardness values, Hv, were recorded across randomly selected diameters at the mid-sectional planes parallel to the upper surfaces on the vertical cross-sections of the Al–Cu disks after HPT for up to 60 turns and on the CP Al and Cu after HPT for 10 turns.

Detailed microstructural analysis was conducted by transmission electron microscopy (TEM) using a JEOL JEOM-2100F after HPT for 20 and 60 turns. The TEM specimens were taken at a distance of 1 mm from the edges of the processed disks and specimens were prepared using a focused ion beam, FEI Quanta 3D FEG. Compositional maps were obtained using energy dispersive spectroscopy (EDS) in a scanning TEM mode. The overall compositions and phase analyses were conducted by X-ray diffraction (XRD) with a Rigaku Ultima III using Cu Kα radiation at a scanning speed of 0.5 min^{-1} and a step interval of 0.01° on slightly polished disk surfaces of the Al–Cu systems after HPT for 20 and 60 turns. Phase identifications and percentages were quantified using XRD data analysis software, Materials Analysis Using Diffraction (MAUD),[31] which is based on the Rietveld method.

The wear properties of the processed Al–Cu metals were measured using a Hanmi STM-Smart tribology tester with a sliding test method at RT. A steel ball with a composition of 0.10–0.15 C, 0.3–0.60 Mn, 0.04 P, 0.04 S (wt%) was used as the counter material with a Rockwell HRC hardness of 58–60. Following the procedure demonstrated earlier,[32] the sliding test was conducted at a distance of 1.0 mm from the edge of each disk at a constant normal load ranging from 10 to 60 N. Totals of eight tests were available on each disk and at least three tests were performed under each testing condition to obtain results having good levels of accuracy. The counter material was sliding at a speed of 0.002 m s^{-1} at 1 and 5 Hz with a stroke of 2.0 mm for a total distance of 100 m. The morphology of the worn surface was examined using a Nanosystemz Co. NV-1000 optical interferometer and a JEOL JCM 5700 scanning electron microscope (SEM). After testing, the samples were cleaned in an ultrasonic bath and the weight losses were measured to estimate the wear coefficients.

3. Experimental Section

3.1. Direct Bonding of Al and Cu Disks

The stacked Al and Cu disks were processed by HPT through 10, 20, 40, and 60 turns and optical micrographs taken on the cross-sections are shown in **Figure 1**a with the measured hardness values along the disk diameters, as shown in Figure 1b. In Figure 1a, the phase with bright color denotes the Al-rich phase, the dark regions correspond to the Cu-rich phase and the gray color at the disk edges relates to a mixture of Al and Cu. It is readily apparent that the upper Al–Cu disk processed through 10 turns gave a multi-layered microstructure over a wide region from the disk center toward $r \approx 3$–4 mm and a mixture of very fine Cu phases within the Al matrix in the remainder at the disk edge where r is a radius of the disk. The central regions with larger Al and Cu phases become smaller with increasing numbers of turns to 20 and 40. Furthermore, additional HPT to 60 turns significantly reduces the multi-layered region at the disk center to $r < 2$ mm and there is a wide peripheral region showing a complete mixture of Al and Cu.
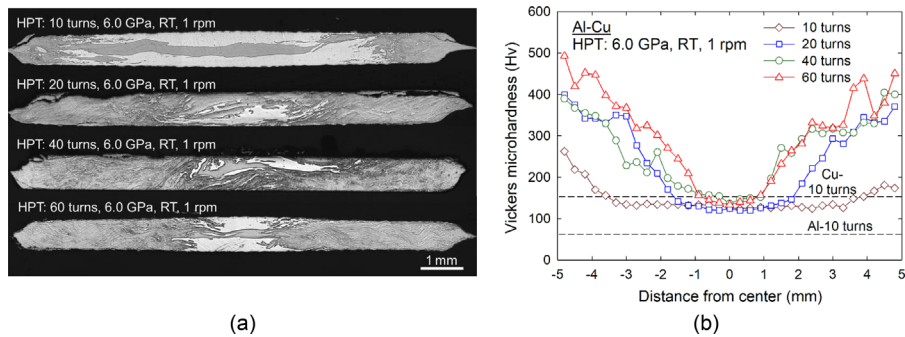
**ADVANCED
SCIENCE NEWS**

www.advancedsciencenews.com

**ADVANCED
ENGINEERING
MATERIALS**

www.aem-journal.com

Figure 1. Stacks of CP, Al, and Cu disks were processed by HPT for 10, 20, 40, and 60 turns. The optical micrographs taken at the cross-sections are shown in a) and the measured hardness values along the disk diameters are shown in b).

The variations of the measured hardness are shown in Figure 1b where the hardness of the base materials of Al and Cu after 10 HPT turns are denoted by the dashed lines at Hv ≈ 65 and Hv ≈ 150, respectively. The central regions of $r < 3$–4 mm after 10 turns, $r < 1$–2 mm after 20 turns, and $r < 1$ mm after 40 and 60 turns show low hardness values of Hv < 150 which are consistent with the hardness of Cu when processed separately by HPT for 10 turns. By contrast, the hardness values in the peripheral regions are exceptionally high with maximum values of Hv ≈ 250, 400, and 500 with increasing numbers of turns to 10, 20–40, and 60, respectively. Although the numbers of HPT turns applied in these experiments are different, the results show a consistent trend of microstructural and hardness evolution with increasing numbers of HPT turns as reported earlier for the Al–Mg system when processing by HPT.[23–26]

3.2. Microstructure and Phase Analysis

Detailed observations of the microstructures were conducted at numbers of locations on the disk edges at $r ≈ 4$ mm at the vertical cross-sections of the Al–Cu metals after HPT for 20 and 60 turns. **Figure 2** shows 1) a representative TEM micrograph, 2) the corresponding diffraction ring pattern, and 3) the EDS

micrographs overlapped with the elemental mapping of Al in green and Cu in red for the Al–Cu disk edges after HPT for 20 turns. Thus, the deformed microstructure consists of ultrafine layers with average thicknesses of ≈20 nm and these layers contain numerous dislocations which subdivide the layers in a vertical sense so that the average grain cell size is ≈80 nm. The presence of Al_2Cu was observed in the diffraction pattern as shown in Figure 2b. It should be noted that the plane of the possible intermetallic phase was identified by confirming both d-spacing and the complementary angles between the standard points of Al and Cu and the intermetallic phases. The EDS micrograph in Figure 2c directly captures the turbulent flow of the ultrafine phases of Al and Cu where this is an inherent feature of processing by torsional straining. Thus, the two phases are mixed without any segregation. In addition, although not all interfaces of the phase mixture at the disk edge presented intermetallic phases during the numbers of TEM observations, a series of point chemical analyses confirmed the presence of Al_2Cu, $AlCu$, and Al_4Cu_9 intermetallic compounds within the measurement region (see supplementary material 1).

A necking and fracturing of the Cu phase when bonding with the Al phase was often observed under simple severe shear when processing by accumulative roll bonding (ARB)[28,33,34] due to the
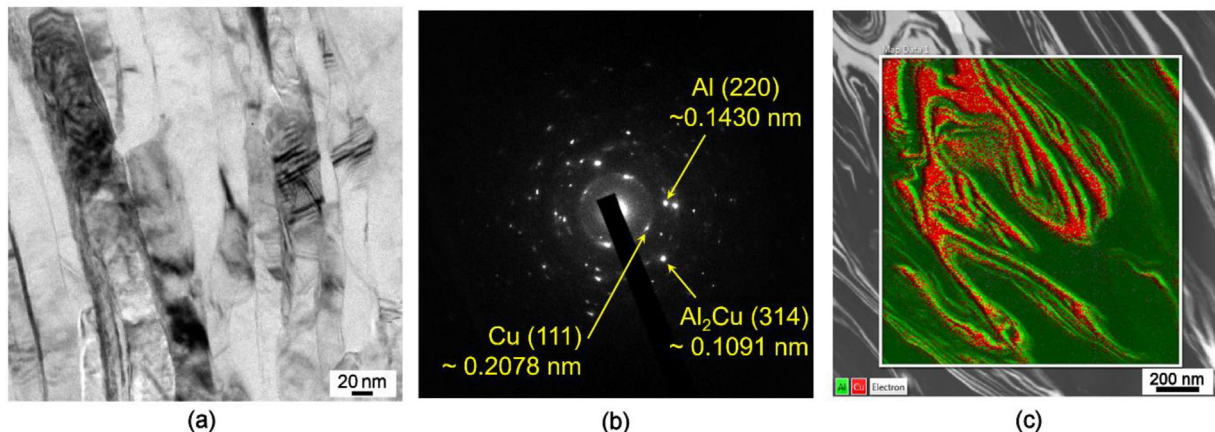

Figure 2. a) A representative TEM micrograph, b) the corresponding diffraction ring pattern, and c) the EDS micrographs overlapped with the elemental mapping of Al in green and Cu in red for the Al–Cu disk edges after HPT for 20 turns.

differences in the stacking fault energies of Al and Cu which produces a large difference in the strain hardening rates of these two phases. Thus, it is anticipated that a unique two-phase turbulent flow will occur in the present study, in addition to necking and fracturing of the Cu in the Al matrix, because of the complex severe shearing under the torsional and compressional straining during HPT processing.

Detailed microstructures in the Al–Cu system after HPT for 60 turns are shown in **Figure 3** where the EDS micrographs and the elemental mapping of Al and Cu at the corresponding area are shown in (a)–(c), respectively, and a representative TEM micrograph and the corresponding diffraction ring pattern are shown in (d) and (e), respectively. It is apparent from the EDS micrographs that after 60 HPT turns the Cu-rich phase is fully dissolved into the Al matrix and there is no evidence for the Cu-rich phase near the disk edge. A number of point chemical analyses demonstrated that all three intermetallic phases of Al_2Cu, $AlCu$, and Al_4Cu_9 were present in the consistent measurement region at the disk edge after 60 turns (See supplementary material 2). Very significant grain refinement was also achieved after 60 HPT turns so that true nano-scale

grains with an average grain size of ≈ 30 nm were observed in an equiaxed microstructure, as shown in Figure 3d. Due to the significant grain refinement, most diffraction spots are presented as rings in Figure 3e. However, a close examination identified the specific points as the specific intermetallic phase planes in the diffraction pattern. Thus, the selected specific diffraction points are marked as yellow circles and the presence of the three different intermetallic compounds is confirmed complementarily by the diffraction pattern, as shown in Figure 3e.

The results of the X-ray analysis are shown in **Figure 4** where the X-ray profiles are given for the disk edges of the Al–Cu system after 20 turns (lower) and 60 turns (upper). Further compositional analyses based on the X-ray profiles were conducted through MAUD and the results are displayed in **Table 1**. For better accuracy in the MAUD analysis, three elements of Al, Cu, and Al_2Cu which are expected to have the highest volume fractions are considered in the analysis but the two other intermetallic phases of AlCu and Al_4Cu_9 are excluded from the analysis because of their similarities to specific peak angles with Al and Cu. The XRD peaks are broadened in Figure 4
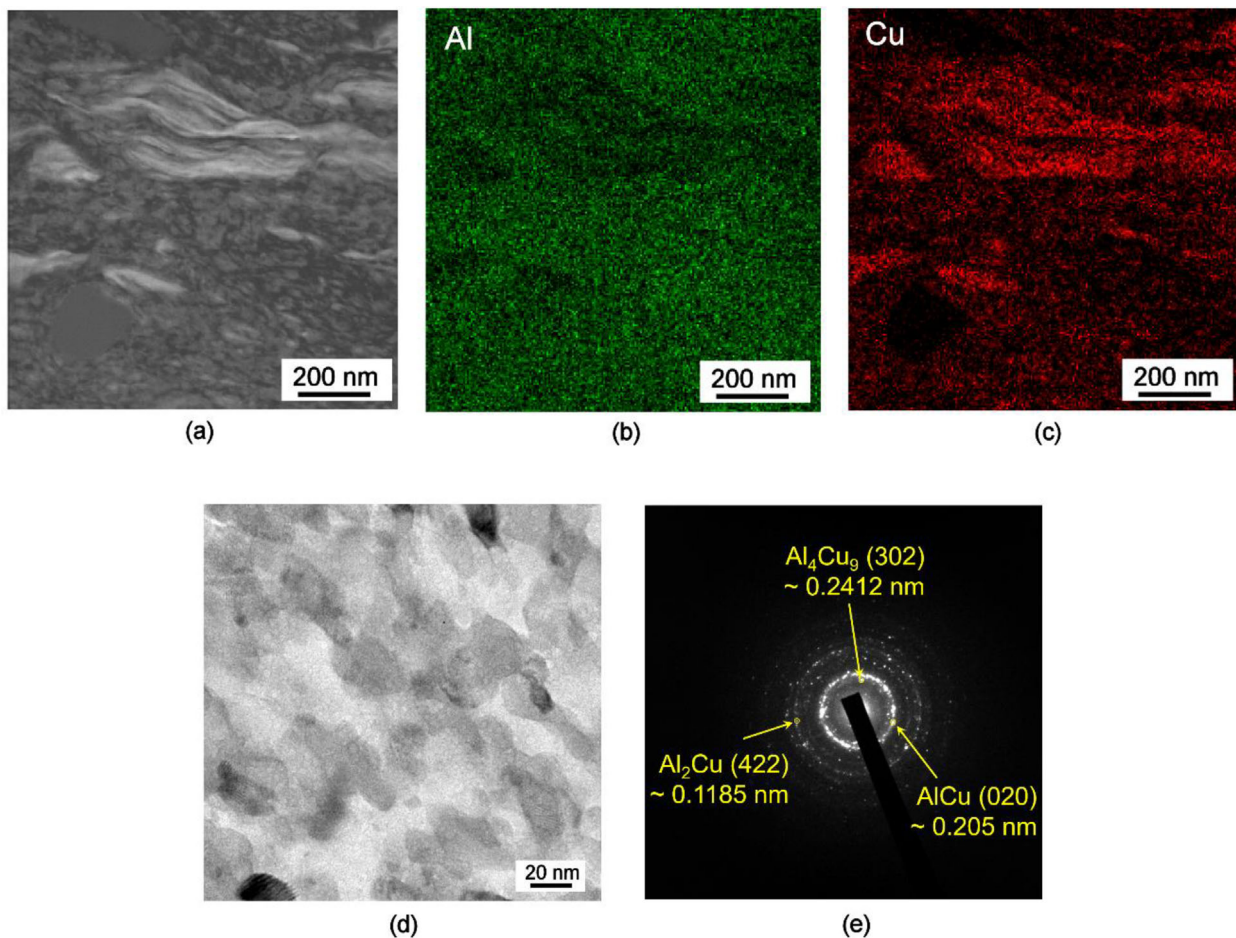

Figure 3. The detailed microstructures in the Al–Cu system after HPT for 60 turns where the EDS micrographs and the elemental mapping of Al and Cu in the corresponding area are shown in a–c), respectively, and a representative TEM micrograph and the corresponding diffraction ring pattern are shown in d) and e), respectively.
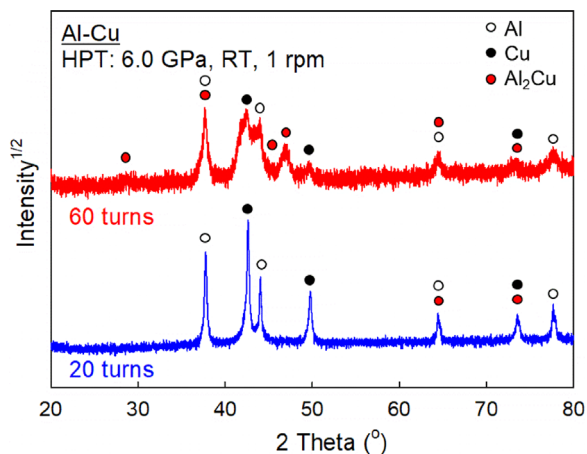
Figure 4. X-ray profiles for the disk edges of the Al–Cu system after 20 turns (lower) and 60 turns (upper).

due mainly to the increasing grain refinement with increasing numbers of HPT turns from 20 to 60. It should be noted that, although only an estimation of Al_2Cu is available in the quantitative analysis, increasing volumes of the intermetallic phases are demonstrated with increasing numbers of HPT turns. Thus, the results confirm that processing by HPT for over 20 turns leads to the successful bonding of Al and Cu throughout the disk sample surfaces and further produces SPD-induced metal-matrix nanocomposites (MMNCs) containing different amounts of intermetallic compounds at the disk edges of the Al–Cu system. The observed Cu of <10 vol% after 60 turns in Table 1 is due to the inclusion of the Cu-rich phase which exists close to the mid-radius of the disk.

3.3. Tribology Tests and Worn Surface Morphology

A series of small-scale sliding tests was conducted to examine the wear properties at the Al–Cu disk edges after HPT for 20 and 60 turns under loads of 10–60 N for total sliding distances of 8.0 m using strokes of $2\,mm\,s^{-1}$ with 1 and 5 Hz. These sliding tests demonstrated there is no significant difference in the measured average coefficients of friction (COF) For example, representative average COF values measured under testing conditions of 30 and 60 N with 1 Hz are listed in **Table 2** after HPT for 20 and 60 turns. The recorded values of the COF were reasonably

Table 1. Results on compositional analysis through MAUD based on the X-ray profile shown in **Figure 4**.

	Volume fraction	
	20 turns	60 turns
Al	0.507 ± 0.052	0.251 ± 0.041
Cu	0.444 ± 0.036	0.099 ± 0.023
Al_2Cu	0.049 ± 0.0	0.650 ± 0.0

Table 2. The recorded friction coefficients under the forces of 30 and 60 N for the Al–Cu system after HPT for 20 and 60 turns.

	Coefficient of friction	
	30 N	60 N
20 turns	0.41 ± 0.06	0.39 ± 0.04
60 turns	0.40 ± 0.04	0.43 ± 0.05

consistent under all sliding conditions for these samples as is apparent from Table 1. It should be noted that, as outlined in some earlier reports,[35,36] the value of the COF does not indicate directly the wear resistance and a further estimate of the wear rate and/or the specific wear rate is required in order to fully evaluate the wear resistance of the Al–Cu system.

Representative morphologies were evaluated by taking the worn surfaces and the results are shown in **Figure 5** where SEM micrographs of the worn surfaces (upper row) and three-dimensional depth-sensing photos at vertical sections in the middle of the wear tracks (lower row) are displayed for the Al–Cu system after HPT through (a) and (c) 20 turns and (b) and (d) 60 turns after testing in wear at 30 N with 1 Hz; the color key beside each depth-sensing plot denotes the detailed depth information. Comparing the SEM micrographs in Figure 5a and b, it is apparent that the processed Al–Cu system after 60 HPT turns exhibits much less wear track volume than the material after 20 turns. Specifically, it is evident from the depth-sensing photos in Figure 5c and d that there is a wider width of >60 μm and larger depth of >8.0 μm at the worn trace after 20 turns by comparison with the worn track width and depth after 60 turns of <30 μm and <3.0 μm, respectively. However, both samples show wear debris, especially at the end of the sliding tracks as in Figure 5a and b, thereby demonstrating an adhesive wear behavior in the Al–Cu system. Several earlier studies demonstrated changes in the wear mechanisms of simple metals such as Ti after grain refinement by HPT[36] and ECAP.[37] Nevertheless, the present results confirm that there is no change in the wear mechanism during microstructural refinement with increasing HPT turns and an increase in the volume of the Al–Cu intermetallic phases in the MMNC at the disk edges of the Al–Cu system.

4. Discussion

4.1. Formation of Al–Cu Intermetallic Compounds through HPT

Several earlier studies reported the formation of some or all of the Al_2Cu, AlCu, and Al_4Cu_9 intermetallic phases after the cold roll-bonding of tri-layered Cu/Al/Cu plates,[38] friction stir welding (FSW) of Al and Cu plates,[39,40] and HPT on semi-circular Al and Cu disks.[20] However, besides the hot working processes by hot-rolling[41,42] and hot hydrostatic extrusion,[43] an additional annealing treatment is often necessary to introduce these intermetallic phases at the Al and Cu interfaces after ARB,[33] cold rolling,[44–46] explosive welding,[47] and FSW.[48] The
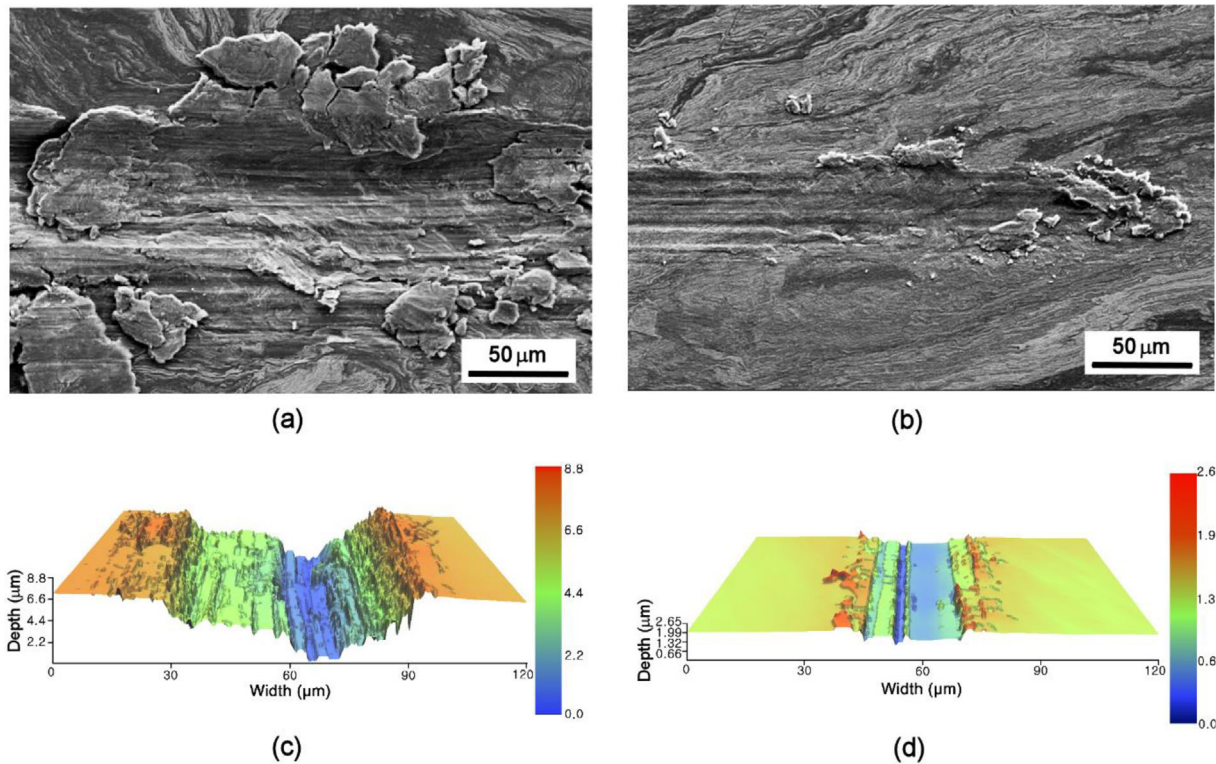
Figure 5. SEM micrographs of the wear surfaces (upper row) and three-dimensional depth-sensing photos at vertical sections in the middle of the wear tracks (lower row) after testing in wear at 30 N with 1 Hz for a) and c) the Al–Cu system after HPT for 20 turns and b) and d) after 60 turns.

intermetallic phases of Al_2Cu and Al_4Cu_9 are the favorable phases to be formed adjacent to the Al-rich and Cu-rich domains, respectively, during an Al/Cu bulk reaction at 300–600 K through interfacial and grain boundary diffusion.[49] It is also supported by a Gibbs free energy calculation that the formation of Al_2Cu is the most favorable followed by Al_4Cu_9, and under the ideal compositional concentrations of Al and Cu then AlCu is the third phase to be formed at $\approx$723 K.[50] Thus, the formation of three intermetallic phases in the present study may be anticipated by the fast atomic diffusion in bulk metals processed by HPT[20,24,51] and a recent review describes the significance of the enhanced atomic mobility during SPD by recognizing the very significant increase in the vacancy concentration within the processed bulk materials.[52]

It should be noted that a temperature increase during HPT processing is critical in terms of atomic diffusion. However, in practice a very recent report demonstrated very limited temperature increases in the very early stages of HPT processing and a saturation at <1 turn under 2.0 GPa for several metals including Al, Ag, Cu, Fe, Sn, and Ti.[53] Moreover, an earlier study on processing of Al and Mg disks by HPT also showed only a limited temperature increase up to 10 HPT turns at 6.0 GPa.[23] Therefore, it is reasonable to consider that the fast atomic diffusivity in the present HPT-processed system may be fully attributed to the severe microstructural distortion which introduces a high population of lattice defects in the nanostructure.

The present experiments demonstrate an excellent capability for using the HPT procedure to achieve a direct bonding and complex mixing of dissimilar metals as an RT manufacturing technique, thereby providing an important contribution to current developments in diffusion bonding, welding and mechanical joining technologies.[54] Furthermore, the HPT processing may be used to form heterostructured nanomaterials[55] involving heterogeneous and gradient microstructures[56,57] in terms of grains, phases and compositions from the sample surfaces to within the bulk solids. This provides a new class of bulk engineering materials with a high potential for exhibiting excellent mechanical properties and functionalities.[58–60] Accordingly, further studies of such unique nanostructured materials will be needed to extend the capabilities and the future applications of bulk nanostructured materials processed by SPD techniques.

4.2. Improvement in Wear Resistance with Increasing HPT Turns

The morphologies of the wear tracks in Figure 5 show that both the depth and width of the wear scars became nearly one-third smaller when increasing the torsional straining from 20 to 60 turns at the disk edges of the Al–Cu MMNCs when testing under a load of 30 N. Thus, the total volume loss during sliding wear is less in the material experiencing increasing numbers of HPT turns, thereby demonstrating higher wear resistance under the testing load.

Further evaluation was conducted to investigate the changes in wear properties with increasing applied load in the HPT-processed Al–Cu system. Specifically, the wear rate, w_R, was estimated by measuring the wear volume, V, and applying the sliding distance, L, in the following form:

$$w_R = \frac{V}{L}, \tag{1}$$

In practice, the specific wear rate, k, may be calculated from Archard's equation[61]:

$$k = \frac{V}{PL} = \frac{W}{PL\rho}, \tag{2}$$

where P is the normal load, W is the weight loss, and ρ is the density of the material.

Table 3 lists the measured weight losses and the estimated wear rates and specific wear rates under applied loads of 30–60 N for the Al–Cu disk edges where the densities were carefully measured as 4.466 and 4.321 g cm^{-3} for the sample edges after 20 and 60 HPT turns, respectively. It should be noted that the sliding tests were conducted at applied loads of 10–60 N, but the low loads of 10 and 20 N provided no measurable amount of weight loss in the alloy system after HPT for both 20 and 60 turns. For reference, the separate materials show densities for the Al disk of 2.73 g cm^{-3}[26] and for the Cu disk of 8.51 g cm^{-3} both after sufficient straining by HPT for 10 turns. Thus, the direct bonding of Al and Cu and the nucleation of new intermetallic phases by HPT introduces excellent lightweight characteristics in the new metal system.

Both wear rate and the k values are lower for the material after 60 HPT turns at all wear loads than after 20 HPT turns, but there is a continuous increase in these values with increasing applied loads. This change in the wear rate with increasing applied load is documented in **Figure 6** for the Al–Cu system for the conditions of 20 and 60 HPT turns. A close evaluation shows there is a large increase in the wear rate at ≈30 N for the Al–Cu system after 20 HPT turns and this increase shifts to ≈50 N after HPT for 60 turns, thereby confirming an improvement in wear resistance by extending the range of the applied load and introducing a lower wear rate. An earlier report examined the specific wear rate and defined mild-wear as in the range of 10^{-5} mm^3 N^{-1} m^{-1} while severe-wear ranges were 10^{-4}–10^{-2} mm^3 N^{-1} m^{-1}.[62] Using these definitions, it follows from the data in Table 3 that all Al–Cu
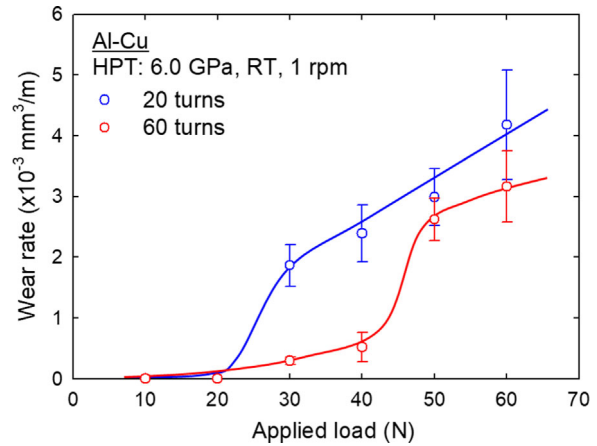

Figure 6. The change in wear rate with increasing applied load for the Al–Cu system after 20 and 60 HPT turns.

samples in the present study exhibit reasonable mild- to intermediate-wear without any severe-wear behavior.

Numerous earlier studies demonstrated that several technical parameters influence the wear properties of ultrafine-grained and nanocrystalline materials, such as the load levels,[37,63–66] the sliding distance,[64,67–70] and the sliding velocity.[37,71] Although it is difficult to directly compare the present data with these earlier reports, a review of the available wear property data of some UFG metals processed by SPD provides a reasonable evaluation of the wear properties of the Al-Cu system. Thus, the computed specific wear rates are $k \approx 9.0 \times 10^{-5}$ mm^3 N^{-1} m^{-1} for a commercial purity Al after accumulative roll bonding for 8 cycles (estimated from $w_R := 1.0 \times 10^{-3}$ mm^3 m^{-1} at 11.2 N),[68] $k \approx 4.2 \times 10^{-5}$ mm^3 N^{-1} m^{-1} for a Cu–Al–Fe alloy after ECAP for 2 passes (estimated from $w_R = 2.5 \times 10^{-3}$ mm^3 m^{-1} at 60 N),[64] $k \approx 6.7 \times 10^{-5}$ mm^3 N^{-1} m^{-1} for a Cu–Zr alloy after ECAP for 8 passes (estimated from $w_R = 1.0 \times 10^{-3}$ mm^3 m^{-1} at 15 N),[71] and $k \approx 1.2 \times 10^{-4}$ mm^3 N^{-1} m^{-1} for Ti after ECAP for 8 passes (estimated from $w_R = 4.0 \times 10^{-3}$ mm^3 m^{-1} at 35 N).[37] By comparison, the present Al–Cu system processed by HPT demonstrated similar or even lower k values than these UFG metals under high wear loads. Therefore, the present results provide a clear demonstration of the excellent wear resistance experienced in the Al–Cu system up to very high applied loads by direct comparison with other documented UFG metals.

Table 3. The measured weight loss and the estimated specific wear rate at the load of 30–60 N and the sliding distance of 100 m at the edges of the Al–Cu system after HPT for 20 and 60 turns.

Load [N]	20 turns [Density: 4.466 g cm^{-3}]			60 turns [Density: 4.321 g cm^{-3}]		
	Weight loss [g]	Wear rate [×10^{-3} mm^3 m^{-1}]	Specific wear rate [×10^{-5} mm^3 N^{-1} m^{-1}]	Weight loss [g]	Wear rate [×10^{-3} mm^3 m^{-1}]	Specific wear rate [×10^{-5} mm^3 N^{-1} m^{-1}]
30	0.00083	1.866	6.220	0.00014	0.293	0.977
40	0.00107	2.388	5.971	0.00038	0.521	1.302
50	0.00133	2.985	5.971	0.00113	2.623	5.246
60	0.00187	4.180	6.967	0.00117	3.163	5.272

5. Summary and Conclusions

1) A successful direct bonding and complex mixing of Al and Mg disks was demonstrated using conventional HPT processing at 6.0 GPa for up to 60 turns at room temperature. The deformed microstructure, phase compositions, hardness, and tribological properties were examined to evaluate the feasibility of using HPT for the formation of a unique Al–Cu system having improved properties of hardness and surface wear.

2) The microstructure after HPT demonstrated an ultrafine-layered structure with an average grain cell size of ≈ 80 nm after 20 HPT turns and an equiaxed microstructure with an average grain size of ≈ 30 nm after 60 turns at the disk edges in the Al–Cu system. At the same time there remained relatively large Al-rich and Cu-rich phases within the disk central regions. The presence of three intermetallic compounds of Al_2Cu, $AlCu$, and Al_4Cu_9 were observed at the disk edges after 20 HPT turns and there was an increasing volume fraction of these phases with increasing numbers of HPT turns. This new metal forming technique, involving the presence of intermetallic phases, leads to the synthesis of MMNCs in the Al-Cu system with an exceptional Vickers microhardness of $Hv \approx 500$ recorded after HPT through 60 turns.

3) Small-scale sliding tests showed a low wear rate of $\approx 1.0 \times 10^{-3}$ mm^3 m^{-1} until ≈ 30 N after 20 HPT turns and this extended to ≈ 50 N after 60 HPT turns, thereby demonstrating the excellent wear resistance of the MMNC in the Al–Cu system. Under appropriate testing conditions, all HPT samples demonstrated mid- to intermediate-wear without any severe-wear behavior. Excellent lightweight characteristics were confirmed by the reduction in density by the formation of MMNCs at the disk edges in the Al–Cu system with increasing numbers of HPT turns.

4) The results demonstrate there is a considerable potential for using conventional HPT processing for the bonding of dissimilar metals as a manufacturing technique and for the development of new alloy systems and ultimately the formation of MMNCs. The microstructures formed by HPT define the material as a heterostructured gradient nanomaterial with a high potential for exhibiting excellent mechanical properties and functionalities.

Supporting Information

Supporting information is available from Wiley Online Library or from the author.

Conflict of Interest

The authors declare no conflict of interest.

[1] R. Z. Valiev, R. K. Islamgaliev, I. V. Alexandrov, *Prog. Mater. Sci.* **2010**, *45*, 103.
[2] R. Z. Valiev, Y. Estrin, Z. Horita, T. G. Langdon, M. J. Zehetbauer, Y. T. Zhu, *Mater. Res. Lett.* **2016**, *4*, 1.
[3] A. P. Zhilyaev, T. G. Langdon, *Prog. Mater. Sci.* **2008**, *53*, 893.
[4] T. G. Langdon, *Acta Mater.* **2013**, *61*, 7035.
[5] A. V. Korznikov, O. Dimitrov, G. F. Korznikova, J. P. Dallas, A. Quivy, R. Z. Valiev, A. Mukherjee, *Nanostruct. Mater.* **1999**, *11*, 17.
[6] N. V. Kazantseva, N. V. Mushnikov, A. G. Popov, P. B. Terent'ev, V. P. Pilyugin, *J. Alloys Compd.* **2011**, *509*, 9307.
[7] B. Srinivasarao, A. P. Zhilyaev, R. Muñoz-Moreno, M. T. Pérez-Prado, *J. Mater. Sci.* **2013**, *48*, 4599.
[8] H. Shahmir, M. Nili-Ahmadabadi, Y. Huang, T. G. Langdon, *J. Mater. Sci.* **2014**, *49*, 2998.
[9] H. Shahmir, M. Nili-Ahmadabadi, Y. Huang, J. M. Jung, H. S. Kim, T. G. Langdon, *Mater. Sci. Eng. A* **2015**, *626*, 203.
[10] J.-K. Han, X. Li, R. Dippenaar, K.-D. Liss, M. Kawasaki, *Mater. Sci. Eng. A* **2017**, *714*, 84.
[11] Y. T. Zhu, T. C. Lowe, T. G. Langdon, *Scr. Mater.* **2004**, *51*, 825.
[12] A. P. Zhilyaev, A. A. Gimazov, G. I. Raab, T. G. Langdon, *Mater. Sci. Eng. A* **2008**, *486*, 123.
[13] K. Edalati, Y. Yokoyama, Z. Horita, *Mater. Trans.* **2010**, *51*, 23.
[14] A. V. Korznikov, I. M. Safarov, D. V. Laptionok, R. Z. Valiev, *Acta Metall. Mater.* **1991**, *39*, 3193.
[15] V. V. Stolyarov, Y. T. Zhu, T. C. Lowe, R. K. Islamgaliev, R. Z. Valiev, *Mater. Sci. Eng. A* **2000**, *282*, 78.
[16] K. Edalati, Z. Horita, H. Fujiwara, K. Ameyama, *Metall. Mater. Trans. A* **2010**, *41A*, 3308.
[17] J. M. Cubero-Sesin, Z. Horita, *Mater. Sci. Eng. A* **2012**, *558*, 462.
[18] Y. Zhang, S. Sabbaghianrad, H. Yang, T. Topping, T. G. Langdon, E. J. Lavernia, J. M. Schoenung, S. Nutt, *Metall. Mater. Trans. A* **2015**, *46A*, 5877.
[19] A. P. Zhilyaev, G. Ringot, Y. Huang, J. M. Cabrera, T. G. Langdon, *Mater. Sci. Eng. A* **2017**, *688*, 498.
[20] K. Oh-Ishi, K. Edalati, H. S. Kim, K. Hono, Z. Horita, *Acta Mater.* **2013**, *61*, 3482.
[21] O. Bouaziz, H. S. Kim, Y. Estrin, *Adv. Eng. Mater.* **2013**, *15*, 336.
[22] X. Qiao, X. Li, X. Zhang, Y. Chen, M. Zheng, I. S. Golovin, N. Gao, M. J. Starink, *Mater. Lett.* **2016**, *181*, 187.
[23] B. Ahn, A. P. Zhilyaev, H.-J. Lee, M. Kawasaki, T. G. Langdon, *Mater. Sci. Eng. A* **2015**, *635*, 109.
[24] M. Kawasaki, B. Ahn, H.-J. Lee, A. P. Zhilyaev, T. G. Langdon, *J. Mater. Res.* **2016**, *31*, 88.
[25] B. Ahn, H.-J. Lee, I.-C. Choi, M. Kawasaki, J.-I. Jang, T. G. Langdon, *Adv. Eng. Mater.* **2016**, *18*, 1001.
[26] J.-K. Han, H.-J. Lee, J.-I. Jang, M. Kawasaki, T. G. Langdon, *Mater. Sci. Eng. A* **2017**, *684*, 318.
[27] N. Ibrahim, M. Peterlechner, F. Emeis, M. Wegner, S. V. Divinski, G. Wilde, *Mater. Sci. Eng. A* **2017**, *685*, 19.

**ADVANCED
SCIENCE NEWS**

www.advancedsciencenews.com

**ADVANCED
ENGINEERING
MATERIALS**

www.aem-journal.com

[28] M. Eizadjou, A. K. Talachi, H. D. Manesh, H. S. Shahabi, K. Janghorban, *Compos. Sci. Technol.* **2008**, *68*, 2003.

[29] M. Kawasaki, T. G. Langdon, *Mater. Sci. Eng. A* **2008**, *498*, 341.

[30] R. B. Figueiredo, P. R. Cetlin, T. G. Langdon, *Mater. Sci. Eng. A* **2011**, *528*, 8198.

[31] L. Lutterotti, *Nucl. Instrum. Methods Phys. Res. Sect. B* **2010**, *268*, 334.

[32] C. L. Wang, Y. H. Lai, J. C. Huang, T. G. Nieh, *Scr. Mater.* **2010**, *62*, 175.

[33] V. Y. Mehr, M. R. Toroghinejad, A. Rezaeian, *Mater. Sci. Eng. A* **2014**, *601*, 40.

[34] M. Reihanian, M. Naseri, *Mater. Des.* **2016**, *89*, 1213.

[35] C. T. Wang, N. Gao, R. J. K. Wood, T. G. Langdon, *J. Mater. Sci.* **2011**, *46*, 123.

[36] C. T. Wang, N. Gao, M. G. Gee, R. J. K. Wood, T. G. Langdon, *Wear* **2012**, *280*, 28.

[37] P. Q. La, J. Q. Ma, Y. T. Zhu, J. Yang, W. M. Liu, Q. J. Xue, R. Z. Valiev, *Acta Mater.* **2005**, *53*, 5167.

[38] I.-K. Kim, S. I. Hong, *Mater. Des.* **2014**, *57*, 625.

[39] P. Xue, B. L. Xiao, D. R. Ni, Z. Y. Ma, *Mater. Sci. Eng. A* **2010**, *527*, 5723.

[40] C. W. Tan, Z. G. Jiang, L. Q. Li, Y. B. Chen, X. Y. Chen, *Mater. Des.* **2013**, *51*, 466.

[41] X. K. Peng, R. Wuhrer, G. Heness, W. Y. Yeung, *J. Mater. Sci.* **1999**, *34*, 2029.

[42] G. Heness, R. Wuhrer, *Mater. Sci. Eng. A* **2008**, *483–484*, 740.

[43] K. Y. Rhee, W. Y. Han, H. J. Park, S. S. Kim, *Mater. Sci. Eng. A* **2004**, *384*, 70.

[44] M. Abbasi, A. K. Taheri, M. T. Salehi, *J. Alloys Compd.* **2001**, *319*, 233.

[45] L. Y. Sheng, F. Yang, T. F. Xi, C. Lai, H. Q. Ye, *Compos. Part B* **2011**, *42*, 1468.

[46] W. N. Kim, S. I. Hong, *Mater. Sci. Eng. A* **2016**, *651*, 976.

[47] M. Honarpisheh, M. Asemabadi, M. Sedighi, *Mater. Des.* **2012**, *37*, 122.

[48] W.-B. Lee, K.-S. Bang, S.-B. Jung, *J. Alloys Compd.* **2005**, *390*, 212.

[49] H. J. Jang, J. Y. Dai, H. Y. Tong, B. Z. Ding, Q. H. Song, Z. Q. Hu, *J. Appl. Phys.* **1993**, *74*, 6165.

[50] Y. Wei, J. Li, J. Xiong, F. Zhang, *Eng. Sci. Technol. Int J.* **2016**, *19*, 90.

[51] D.-H. Lee, I.-C. Choi, M.-Y. Seok, J. He, Z. Lu, J.-Y. Suh, M. Kawasaki, T. G. Langdon, J.-I. Jang, *J. Mater. Res.* **2015**, *30*, 2804.

[52] S. V. Divinski, G. Reglitz, H. Rösner, Y. Estrin, G. Wilde, *Acta Mater.* **2011**, *59*, 1974.

[53] K. Edalati, Y. Hashiguchi, P. H. R. Pereira, Z. Horita, T. G. Langdon, *Mater. Sci. Eng. A* **2018**, *714*, 167.

[54] K. Martinsen, S. J. Hu, B. E. Carlson, *CIRP Annals* **2015**, *64*, 679.

[55] I. A. Ovid'ko, R. Z. Valiev, Y. T. Zhu, *Prog. Mater. Sci.* **2018**, *94*, 462.

[56] X. L. Wu, P. Jiang, L. Chen, J. F. Zhang, F. P. Yuan, Y. T. Zhu, *Mater. Res. Lett.* **2014**, *2*, 185.

[57] K. Lu, *Science* **2014**, *345*, 1455.

[58] X. L. Wu, P. Jiang, L. Chen, F. P. Yuan, Y. T. Zhu, *Proc. Natl. Acad. Sci. USA* **2014**, *111*, 7197.

[59] Y. Liu, B. Jin, J. Lu, *Mater. Sci. Eng. A* **2015**, *636*, 446.

[60] X. Wu, Y. Zhu, *Mater. Res. Lett.* **2017**, *5*, 527.

[61] J. F. Archard, *J. Appl. Phys.* **1953**, *24*, 981.

[62] K. Hiratsuka, K. Muramoto, *Wear* **2005**, *259*, 467.

[63] V. V. Stlyarov, L. S. Shuster, M. S. Migranov, R. Z. Valiev, Y. T. Zhu, *Mater. Sci. Eng. A* **2004**, *371*, 313.

[64] L. L. Gao, X. H. Cheng, *Wear* **2008**, *265*, 986.

[65] T. Kucukomeroglu, *Mater. Des.* **2010**, *31*, 782.

[66] K. Edalati, M. Ashida, Z. Horita, T. Matsui, H. Kato, *Wear* **2014**, *310*, 83.

[67] Z. N. Farhat, Y. Ding, D. O. Northwood, A. T. Alpas, *Mater. Sci. Eng. A* **1996**, *206*, 302.

[68] A. K. Talachi, M. Eizadjou, H. D. Manesh, K. Janghorban, *Mater. Charact.* **2011**, *62*, 12.

[69] E. Ortiz-Cuellar, M. A. L. Hernandez-Rodriguez, E. García-Sanchez, *Wear* **2011**, *271*, 1828.

[70] C. T. Wang, N. Gao, M. G. Gee, R. J. K. Wood, T. G. Langdon, *J. Mater. Sci.* **2013**, *48*, 4742.

[71] J. Li, J. Wongsa-Ngam, J. Xu, D. Shan, B. Guo, T. G. Langdon, *Wear* **2015**, *326*, 10.